Drop Impact on a Solid Surface

C. Josserand[1] and S.T. Thoroddsen[2]

[1]Sorbonne Universités, CNRS and UPMC Université Paris VI, UMR 7190, Institut
D'Alembert, F-75005 Paris, France; email: christophe.josserand@upmc.fr

[2]Division of Physical Sciences and Engineering and Clean Combustion Research Center, King
Abdullah University of Science and Technology (KAUST), Thuwal 23955-6900, Saudi Arabia

Keywords

splashing, spreading, bouncing, fingering, air entrapment, roughness,
repellency, superhydrophobicity

Abstract

A drop hitting a solid surface can deposit, bounce, or splash. Splashing arises
from the breakup of a fine liquid sheet that is ejected radially along the sub-
strate. Bouncing and deposition depend crucially on the wetting properties
of the substrate. In this review, we focus on recent experimental and theoret-
ical studies, which aim at unraveling the underlying physics, characterized
by the delicate interplay of not only liquid inertia, viscosity, and surface ten-
sion, but also the surrounding gas. The gas cushions the initial contact; it
is entrapped in a central microbubble on the substrate; and it promotes the
so-called corona splash, by lifting the lamella away from the solid. Particular
attention is paid to the influence of surface roughness, natural or engineered
to enhance repellency, relevant in many applications.

1. INTRODUCTION

The fingering of an ink blot or a coffee stain is familiar to everyone. However, despite 140 years of study (Worthington 1876), the underlying rapid dynamics of the impact process eluded explanation until the past 20 years, when high-speed video technology began to allow time-resolved observations of this intriguing phenomenon (Thoroddsen et al. 2008). The increasing pace of sensor improvements and availability is allowing the study of ever-finer detail and is reinvigorating research in this area of study, as demonstrated by the large number of very recent references cited herein. This imaging technology is now reaching the diffraction limit of spatial resolution and submicrosecond interframe times (Li & Thoroddsen 2015, Visser et al. 2015). This is being matched by increasing computational power and improved numerical algorithms to allow fully resolved simulations in the axisymmetric configuration (Thoraval et al. 2012), and fully three-dimensional (3D) cases, from first contact, should soon follow (Agbaglah et al. 2011).

We strictly confine our review to impacts on solid surfaces and leave out studies involving impacts on pools or films of liquid. Moreover, we emphasize recent works [i.e., appearing after the earlier review by Yarin (2006) in this journal, which dealt with impacts on both solid and liquid surfaces].

Studies of drop impacts are driven by several areas relevant both in nature and in industry. In nature, a drop of water hollows a stone, and splashing produces aerosols, causes erosion, and brings the smell of the earth during rain (Joung & Buie 2015). In industry, there are spray/wall interactions in coating, cleaning, cooling, and combustion. Inkjet droplets play an increasing role in fabrication, from the soldering of electronics to microarrays in biotechnology.

Figure 1 presents some iconic images of impacting drops, including sketches by Worthington around the dawn of photography. He used an ingenious mechanical contraption, with spark
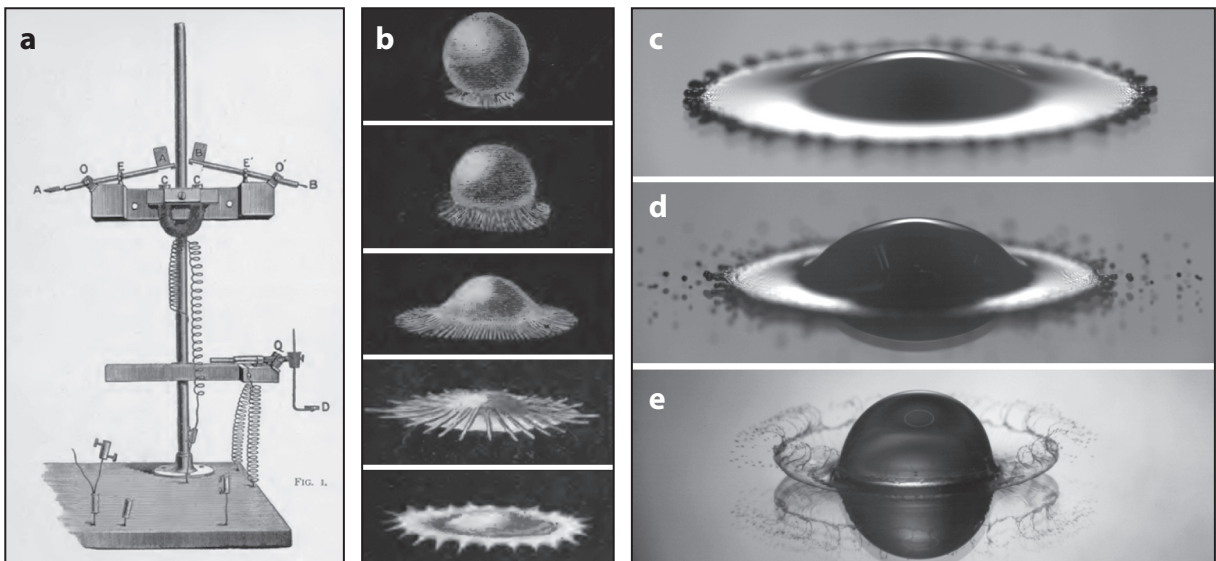
Figure 1

(*a*) Worthington's drop-release setup and (*b*) his sketches of an impacting mercury drop. (*c*) Reproduction of Worthington's impact conditions for mercury on glass using modern video technology. (*d*) Prompt splash for mercury drop impacting superhydrophobized glass. (*e*) Corona splash for ethanol drop on glass. Panels *d* and *e* courtesy of Erqiang Li. Readers are also referred to **Supplemental Videos 1–3** (follow the **Supplemental Material link** from the Annual Reviews home page at **http://www.annualreviews.org**).

Supplemental Material

illumination, triggered by a marble falling in tandem with the drop (**Figure 1a**). He then sketched his flash-illuminated visions of the impact of a mercury drop (**Figure 1b**), with interesting finger-like spokes on the spreading lamella. However, with modern technology, we have reproduced his impact conditions (i.e., 1/15-inch drop diameter and 3-inch impact height) but see no such radial spokes (**Figure 1c**). One possible explanation for the different results involves soot, which Worthington used to superhydrophobize his spectacle glass for releasing the drop (soot also works well as an oleophobic coating; see Deng et al. 2012). This might have formed a coating on the drop; an oxidized layer may have formed; or simply the flash duration was too long and smeared out the edge bumps into radial streaks, as suggested in the celebrated review by Rein (1993).

To define the different parameters involved in drop impacts, we consider as a prototype the normal impact of a spherical liquid drop on a flat solid substrate. The drop diameter is $D = 2R$, and the normal impact velocity is V. The liquid and surrounding gas have densities ρ_ℓ and ρ_g, and dynamical (kinematic) viscosities μ_ℓ ($\nu_\ell = \mu_\ell / \rho_\ell$) and μ_g ($\nu_g = \mu_g / \rho_g$), respectively. The surface tension is denoted by γ and the gravity by g, which is oriented along the vertical direction.

As stated above, the canonical impact problem depends a priori on five dimensionless parameters. In fact, considering the balance between gravity and inertia through the Froude number $Fr = V/\sqrt{gD}$, one can show that gravity can be neglected. Indeed, for usual impact conditions, we find that $Fr \gg 1$ so that only four dimensionless parameters are pertinent for the impact dynamics, although gravity plays a crucial role in the experiment by accelerating the drop until it reaches its impact velocity. In general, the impact dynamics were first characterized by the Reynolds and Weber numbers, defined with the liquid properties as

$$Re = \frac{\rho_\ell DV}{\mu_\ell} \quad \text{and} \quad We = \frac{\rho_\ell DV^2}{\gamma},$$

which balance the inertia with the viscous and the capillary forces, respectively. Alternatively, the Ohnesorge and capillary numbers are often used in the literature, yielding

$$Oh = \frac{\mu_\ell}{\sqrt{\rho_\ell D\gamma}} = \frac{\sqrt{We}}{Re}, \quad \text{and} \quad Ca = \frac{\mu_\ell V}{\gamma}.$$

Additionally, there are the two ratios of the liquid-gas densities and viscosities, ρ_ℓ / ρ_g and μ_ℓ / μ_g. Instead of the use of the viscosity ratio, it is convenient to introduce the Stokes number to quantify the influence of the gas in the lubrication layer beneath the drop before impact:

$$St = \frac{\mu_g}{\rho_\ell DV} = \frac{\mu_g}{\mu_\ell} \cdot \frac{1}{Re}.$$

Finally, other dimensionless parameters can be present in the dynamics, often hidden in the literature, and related to the drop shape (e.g., the aspect ratio of the drop at impact) or the substrate properties (in particular, the contact angle θ_e and roughness distribution).

2. EARLY CONTACT: CENTRAL BUBBLE AND SKATING ON AIR

2.1. Central Bubble

Under atmospheric conditions, a drop impacting perpendicularly to a wall will always entrap a small air bubble under its center. The drop approaches the solid surface inside a gas, which must be displaced before contact. When the drop gets close to the surface, the lubrication pressure in the thin air layer due to the gas viscosity becomes strong enough to deform its bottom into a dimple and thus transform a point contact into one along a ring, with a thin disk of air entrapped. The air disk contracts rapidly into a central bubble on the substrate to minimize the surface energy. This

Reynolds number:
$Re = (\rho_\ell DV)/\mu_\ell$

Weber number:
$We = (\rho_\ell DV^2)/\gamma$

Ohnesorge number:
$Oh = \mu_\ell / \sqrt{\rho_\ell D\gamma}$

Capillary number:
$Ca = (\mu_\ell V)/\gamma$

Stokes number:
$St = \mu_g / (\rho_\ell DV)$

bubble was observed in the snapshots (Chandra & Avedisian 1991, Thoroddsen & Sakakibara 1998) and under inkjet droplets (Van Dam & Le Clerc 2004), but without clear explanation of its formation. Thoroddsen et al. (2005) used high-speed video to directly observe the initial air disk and its contraction. Measuring the volume of air in the resulting bubble, they estimated the initial average thickness of the air disk in the range $\bar{\delta} \sim 2$–5 μm. The contraction speed was successfully modeled with capillary-inertial dynamics by assuming that the layer is uniform but increases in thickness during the reduction in radius. This gives an expression for the disc radius versus time, $R = R_0 \exp[-C\sqrt{\pi\sigma/\rho\Omega_b}\ t]$, in close agreement with the measurements. Here the constant $C \simeq 0.94$, and Ω_b is the bubble volume. However, the edge of the contracting air sheet thickens. Thus, the disk is not of uniform thickness, which is perhaps most clearly visible in the X-ray imaging of Lee et al. (2012). This led Liu et al. (2013) to improve on the above expression, adding corrections to the contraction rate.

Recent advances have used high-speed interferometry to directly measure the radial thickness profile of the air disc. Interferometry fringes can easily give radial changes in the layer thickness, with a resolution of $\lambda/4 \sim 150$ nm between a dark and a bright fringe (Driscoll et al. 2010, Driscoll & Nagel 2011, Liu et al. 2013). However, more sophisticated methods must be applied to obtain absolute thicknesses, including two-color techniques (de Ruiter et al. 2012) and white-light interferometry (van der Veen et al. 2012). Two-color techniques can give extraordinary subfringe thickness resolution, approximately 30 nm (de Ruiter et al. 2015b). These techniques have primarily been applied to low-impact velocities, specifically the study of bouncing dynamics (de Ruiter et al. 2015a). However, with 50-ns laser pulses for each video frame, interferometry can be realized at 5 Mfps (Li & Thoroddsen 2015) to obtain the time-resolved evolution of the air-layer profile for higher impact velocities (**Figure 2c,d**).

The contraction of the air disc into the central bubble also does not come without surprises. Thoroddsen et al. (2005) showed that the retracting edge produces capillary waves, which propagate toward the center. Sometimes the apex of this converging wave touches the substrate at the axis of symmetry and pinches off a microdrop within the central bubble (**Figure 2**). Lee et al. (2012) verified these proposed dynamics using X-ray imaging (**Figure 2b**). Their images even reveal a subsatellite formed inside the bubble inside the drop.

2.2. Modeling the Air-Layer Thickness

The deformation of the bottom of the drop, the formation of the dimple, and subsequent entrapment of the air disc are governed by a balance between the drop's inertia and the lubrication pressure in the air, which tries to escape the oncoming drop. The air-layer cushioning was first modeled by looking at 2D cases (Smith et al. 2003, Korobkin et al. 2008), later adapted to the axisymmetric configuration, which exhibits the same scaling (Hicks & Purvis 2010). Here the dynamics assume viscous lubrication pressure in the air layer, which, for small separation distances, starts to deform the drop inviscidly. These rapid motions can neglect surface tension, liquid viscosity, and gravity. The dimensional argument is essentially the following (Mandre et al. 2009): The separation distance H between the drop and solid must become small enough so that the lubrication pressure in this thin air layer, $P \sim \mu_g VR/H^2$, becomes strong enough to rapidly decelerate the bottom tip of the drop. There, the horizontal/radial scaling used is $\sqrt{DH}$, coming from geometrical arguments. The deceleration a occurs over this distance H, in the very short available time $\tau \sim H/V$, giving $\rho_\ell a \sim \rho_\ell V/\tau \sim \rho_\ell V^2/H$. Equating these two effects gives a characteristic thickness for the start of drop deformation involving the Stokes number, $H^* = R\, St^{2/3}$.
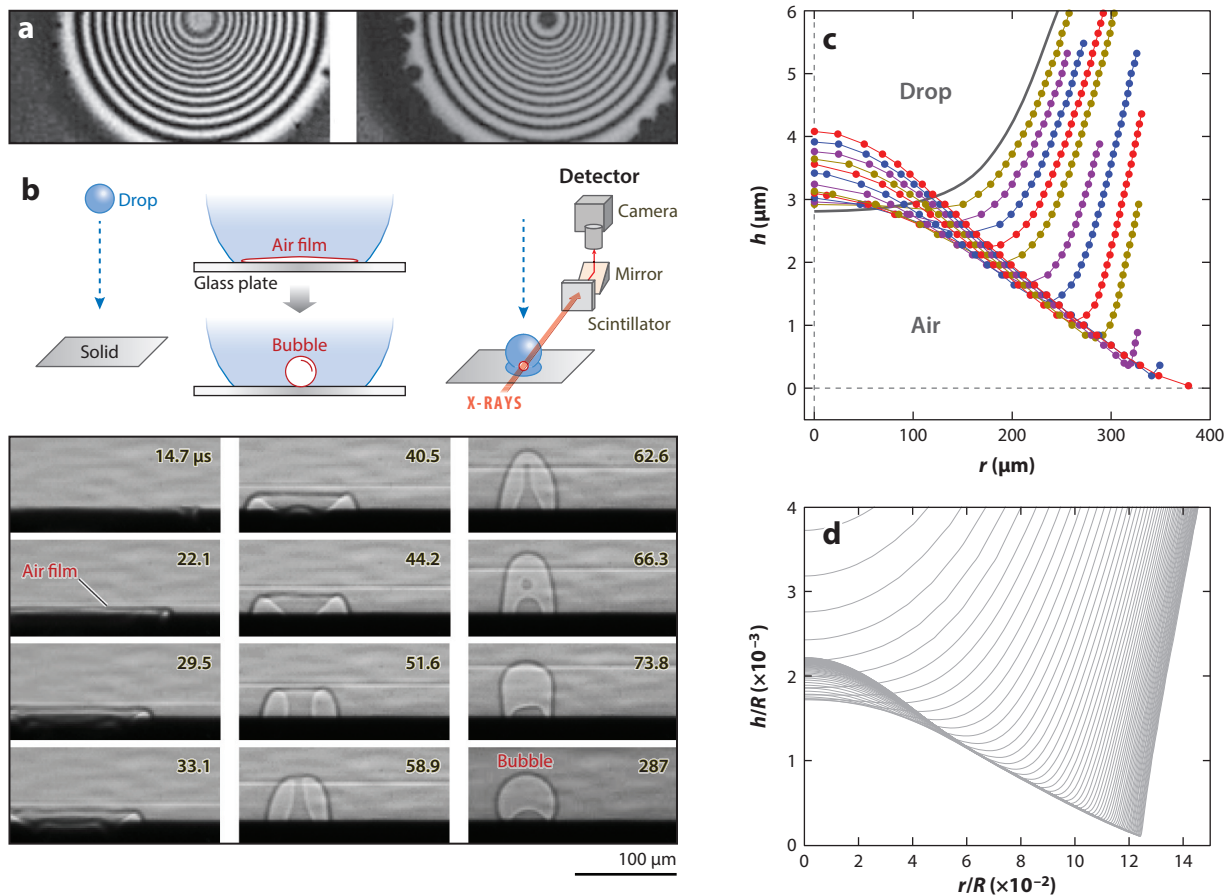
Figure 2

(*a*) Examples of interference patterns of the central air disc. Panel *a* modified with permission from Liu et al. (2013). (*b*) X-ray imaging setup for the entrapment of an air disc and its contraction into an air bubble, with a subsatellite pinched off at its center (Lee et al. 2012). (*c*) Examples of central air-disc shapes during the approach of the drop and contact with the substrate, at impact velocity $V = 1.06$ m/s. Panel *c* adapted from Li & Thoroddsen (2015). (*d*) Same profiles obtained numerically by Duchemin & Josserand (2011). Readers are also referred to **Supplemental Videos 4–6**.

This allowed quantitative comparison to experiments. For example, the prediction of the initial radius of the contact ring (Hicks et al. 2012)

$$L_o = 3.8 \left(\frac{4\mu_g}{\rho_\ell V} \right)^{1/3} R^{2/3} \tag{1}$$

is in reasonable agreement with available data (Liu et al. 2013, Thoroddsen et al. 2005), without any adjustable constants, but one must use the bottom radius of curvature of the falling drop for *R*.

2.3. Gas Compressibility

Building on the previous incompressible theory (Smith et al. 2003, Korobkin et al. 2008), Mandre et al. (2009) found conditions, for higher impact velocities, at which the compressibility of the

gas comes into play. This effect is included in the lubrication equation for the gas in a low–Mach number approximation and is expressed in terms of a compressibility factor

$$\epsilon = \frac{P_{atm}}{(RV^7\rho_\ell^4/\mu_g)^{1/3}}.$$ (2)

If $\epsilon^{-1} \gtrsim 5$, one expects compression of the air disc and smaller values of H^*. This thinning should scale as $H^*/(R_b St^{2/3}) = 3.2\epsilon^{1/3}$. Li & Thoroddsen (2015) recently carried out interferometry experiments for ϵ^{-1} as high as 40, verifying this theory and the corresponding numerics of Mandre et al. (2009) for adiabatic compression. The measured disc thickness, at the centerline, is as thin as $H^* \sim 0.5$ μm.

Hicks & Purvis (2013) added more thermodynamics into the equation of state for the gas. Furthermore, although their compressible theory is limited to two dimensions, they showed that L_o is not dependent on the gas compressibility. This has indeed been borne out by Li & Thoroddsen (2015), who found a perfect fit of L_o to Equation 1, over a large range of impact values, well into the compressible regime. This finding contradicts Liu et al.'s (2013) earlier results, in which smaller water drops were used and L_o was essentially independent of V.

The air film should continue to thin at even higher impact velocities. Indeed, perhaps surprisingly, single central bubbles are observed in the snapshots of Mehdizadeh et al. (2004) for V as high as 40 m/s, where $\epsilon^{-1} \simeq 1,360$ (**Figure 7**). The corresponding air-disc thickness is predicted to be $H^* \simeq 15$ nm, at which stage one might expect molecular forces to break up the air layer before contraction into the bubble.

2.4. Size of the Entrapped Bubble

The size of the entrapped air bubble is important in inkjet-based fabrication, as it can have detrimental effects, for example, on uniformity and conductance. For minuscule impact velocities, the lubricating air film can become unstable and break the axisymmetry, allowing the air to escape (see Klaseboer et al. 2000). The lowest velocities can also lead to isolated contacts and spreading with minimal air entrapment (Kolinski et al. 2012, de Ruiter et al. 2015a). Bouwhuis et al. (2012) applied interferometry to investigate the size of the entrapped air layer and found a maximum, which occurs at a moderate impact velocity, at which compressibility can be ignored. This arises because of competition between the surface tension and inertia of the liquid. For low-enough impact velocities, the surface tension minimizes the drop deformation away from a spherical shape and $H^* \sim St^{1/2}$. At higher velocities, inertia dominates, and the dynamic pressure grows as a square of velocity, thus draining out more air, which reduces $H^* \sim St^{2/3}$, in agreement with the findings of Mandre et al. (2009). Between these two considerations is a maximum, with a crossover at $St_c \sim Ca_g^{3/4}$ [where $Ca_g = (\mu_g V)/\gamma$ is the capillary number based on the gas viscosity] or expressed in a critical impact velocity $V_c \sim (\mu_g \sigma^3 / \rho_\ell^4 R^4)^{1/7}$. For their ethanol drop, with $R = 0.9$ mm, they get $V_c = 0.25$ m/s. Klaseboer et al. (2014) proposed a different power law for the large–impact velocity regime, $H \sim St^{1/2}$, arising from the use of a different velocity potential in the drop than that used by Bouwhuis et al. (2012).

Hendrix et al. (2015) proposed a model unifying three impact configurations—a drop onto a solid, a solid sphere onto a pool (Marston et al. 2011), and a drop onto pool—showing that the normalized bubble volume $V_b/V_{drop} \sim St^{4/3}$. However, for the last configuration, twice as much volume is entrapped, or half the impact velocity must be used, owing to the two compliant surfaces arising from the added mass of the pool.

## 2.5. Skating on a Thin Layer of Air or Contact with the Solid Substrate

One of the interesting questions raised by the above studies is the detailed break of the air layer when molecular contact is first established with the solid substrate. Motivated by the effect of air pressure on splashing, Mandre et al. (2009) suggested that the drop might slide on a continuous layer of air and splash without molecular contact. Kolinski et al. (2012) used total internal reflection to support this notion and coined the phrase "skating on a film of air." This technique observes the gracing light reflected from a glass surface, when the angle between the incident light and glass surface is smaller than a critical angle (48° for air-glass). However, when the liquid makes contact with the glass surface, because of the similar refractive index of the glass and liquid, the reflection disappears, and the contacts become clearly marked by dark spots. Some signature is also observed owing to an evanescent wave, when the air layer becomes a few tens of nanometers, allowing measurements of the bottom profile of the drop (Kolinski et al. 2014a,b).

Following much debate, this issue can be clarified by the following observations. First, the contraction of the central disc into the bubble would not occur without a contact line, which must be present to allow the reduction in surface energy (Thoroddsen et al. 2005). Second, Driscoll & Nagel (2011) used an optical interference technique to show that for higher impact velocities, the liquid contact outside the central disk wets the substrate. Their measurements show that if there were a thin air layer present, it must be less than 3.5 nm thick. Such a layer would of course be highly unstable by van der Waals interactions. Third, Kolinski et al. (2012) clearly demonstrated that isolated wetting contacts formed and that increasing the impact velocity causes a larger number of contacts along the ring bounding the central disc (see also Kolinski et al. 2014a,b; de Ruiter et al. 2015a). One can speculate that even higher velocities will show still more numerous contacts and a transition to what appears similar to a continuous rupture. The characteristic dark ring marking the initial contact radius, seen by Thoroddsen & Sakakibara (1998) and Thoroddsen et al. (2005) and more recently by de Ruiter et al. (2015a), is likely a microbubble signature of this initial contact. The effects of statistical roughness and isolated asperities remain an open question, as discussed by Mani et al. (2010) and Mandre & Brenner (2012). Common features of many of the images of the early contact through glass plates are several isolated contacts (e.g., see Liu et al. 2013). These most likely result from local asperities, which become important when the air-layer thickness reaches down to dozens of nanometers. This needs to be further studied with glass substrates that have been well characterized before the impact. These details will not change the final outcome but would give a strong indication of the actual air-layer thickness when it ruptures, providing hints at the underlying physics, be they hydrodynamic or molecular in nature.

Conversely, for the lowest impact velocities, the drops can indeed glide on a film of air and rebound without contacting the solid substrate, even for hydrophilic surfaces (Kolinski et al. 2014a). This has been studied in great detail by de Ruiter et al. (2015b), who have shown in careful experiments that skating for a water drop is possible only for $V < 0.48$ m/s. Over a range of liquids, this corresponds to a Weber number of $We < 4$, and the minimum thickness observed is $h_{min} \simeq 200$ nm. Furthermore, the scaling for h_{min} derived from the axisymmetric simulations of Duchemin & Josserand (2011) also shows that for impact velocities, of relevance in splashing, the thickness becomes subnanometric. One must therefore conclude that air skating under the center of the drop is irrelevant for the splashing transition, discussed in the next section.

3. LATER DYNAMICS: SPREADING AND REBOUNDING

Later-time dynamics of the impact exhibit different behaviors depending on the impact and substrate parameters, ranging from smooth spreading to splashing, jetting, and rebound. The
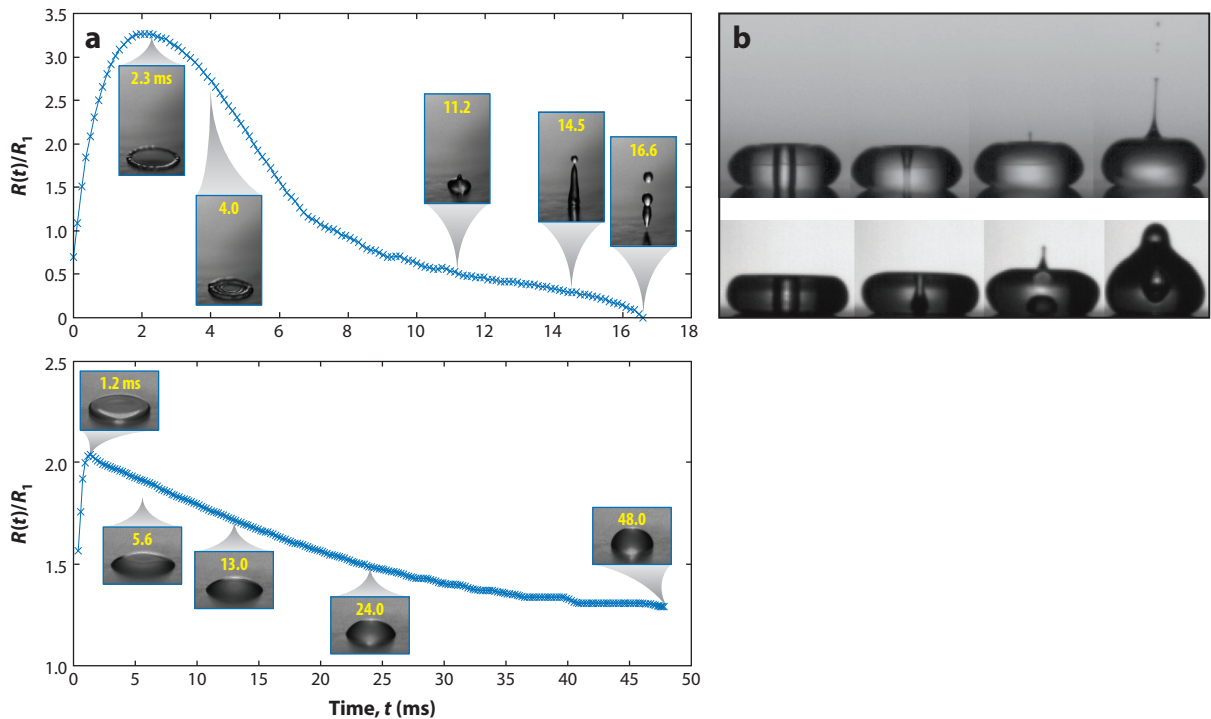
Figure 3

(*a*) Snapshots of spreading and rebounding dynamics as well as the evolution of the spreading radius with time. Panel *a* adapted with permission from Bartolo et al. (2005). (*b*) Singular jet formed by retraction after a small drop impacts on a superhydrophobic surface. Panel *b* taken with permission from Bartolo et al. (2006b).

spreading dynamics are an important aspect in many applications, for instance, for inkjet printing in microelectronics (Minemawari et al. 2011) or in forensic science (Hulse-Smith et al. 2005, Attinger et al. 2013, Laan et al. 2014). In both cases, the splashing-spreading transition is crucial for the printing quality or the determination of the link between the blood pattern and drop trajectories.

3.1. Overall Spreading Dynamics, Rebound, and Jetting

When no splashing is observed, the drop simply spreads over the surface until it reaches a maximum radius. Then, depending on the surface properties, the liquid can recede or remain close to this maximum spread (Rioboo et al. 2001). The dynamics are then controlled by subtle balances between inertia, viscosity, and capillary forces (Bartolo et al. 2005). In particular, when the impact is performed on a (super)hydrophobic surface, the drop's retraction can lead to partial or complete rebound and even to singular jet formation (Renardy et al. 2003, Bartolo et al. 2006b) (**Figure 3**). This occurs through convergence of capillary waves at the apex, which can also entrap bubbles in the drop (Huang et al. 2013). Pittoni et al. (2015) have tracked the various bubble-entrapment mechanisms.

These retraction, rebound, and jetting dynamics can be controlled by varying the wettability of the solid surface (Bayer & Megaridis 2006, Yokoi et al. 2009). This is particularly the case when

the impact is performed on a textured surface. Both the spreading dynamics and the retraction are affected depending whether the liquid penetrates the textured surface (the Wenzel state) or moves over the structures (the Cassie-Baxter state) (Bartolo et al. 2006b, Kwon et al. 2013, Maitra et al. 2014). Furthermore, complex rebound and jetting dynamics can be observed when the drop impacts on an deformable solid surface, such as an elastic membrane (Antkowiak et al. 2011), or on fibers (Piroird et al. 2009), for instance.

3.2. Maximum/Residual Spreading Radius and Minimal Thickness

An important outcome of a drop impact on a solid substrate is the maximum spreading radius. This quantity, pertinent in the absence of splash, has applications in inkjet printing (Minemawari et al. 2011) and forensic science (Hulse-Smith et al. 2005, Attinger et al. 2013), although the crucial quantity in these cases is the residual spreading radius, which can differ from the maximum spreading radius. Numerous relations between the maximum spreading radius (or diameter) and the impact parameters have been established using physical arguments generally based on the balance between inertia and viscous and capillary contributions (Chandra & Avedisian 1991, Pasandideh-Fard et al. 1996, Range & Feuillebois 1998, Rioboo et al. 2002, Roisman et al. 2002, Clanet et al. 2004, Fedorchenko et al. 2005, Ukiwe & Kwok 2005, Roisman 2009, Vadillo et al. 2009, Eggers et al. 2010). It is important to emphasize that all these relations show reasonable agreement with experiments and numerical simulations despite their quite different formulations. Indeed, for the ranges of parameters concerned, the spreading radius does not vary by many orders of magnitude, so power-law scalings are hard to identify, and it is difficult to discriminate between the different models by quantitative arguments alone. Moreover, no asymptotic relation can be tested because of the splashing mechanism that occurs for a large impact velocity, although these relations are often presented in such asymptotic forms. In particular, the initial drop radius is often neglected, so some of these relations should be corrected by subtracting the initial drop radius.

However, most of these models distinguish two regimes for the spreading factor β, defined by the ratio between the maximum radius and the initial one:

$$\beta = \frac{R_{\mathrm{max}}}{R_0}.$$

The first is a viscous regime in which the maximal extension of the drop is obtained using a balance between the kinetic energy and the viscous dissipation. The spreading factor follows the relation $\beta - 1 \propto Re^{1/5}$, often simplified to

$$\beta \propto Re^{1/5}.$$

The second is an inertial regime in which the spreading factor is determined by a more complex balance between the inertia and capillary forces with some correction due to viscous dissipation and wettability effects. Many different models have been proposed in this regime, and their pertinence remained a question of scientific debate until recently. A simple scaling analysis comparing the initial kinetic energy with the surface energy at the maximum spreading radius would suggest an asymptotic regime valid for large Weber numbers, $\beta \propto We^{1/2}$. However, as explained above, the available Weber numbers for this regime in which no splash is present do not really allow one to observe such scaling, and more detailed models have included corrections due to the initial surface energy, contact angle, or viscous dissipation. Clanet et al. (2004) developed an alternative using a mass conservation argument based on the pancake thickness selected by the capillary wave created by the impact and leading to the scaling law $\beta \propto We^{1/4}$. This scaling law has had great success as it gives good quantitative agreement with experimental data for hydrophobic substrates, and it has subsequently been commonly used to fit experimental data. However, we emphasize

Table 1 Different models for the spreading factor β as a function of the impact parameters

| Model	Expression	Comment
Scheller & Bousfield (1995)	$\beta \sim 0.61\,(Re^2\,Oh)^{1/6} = 0.61\,Re^{1/5}(We\,Re^{-2/5})^{1/6}$	Empirical law based on experimental results
Pasandideh-Fard et al. (1996)	$\beta = \sqrt{\dfrac{We+12}{3(1-\cos\theta_a)+4(We/\sqrt{Re})}}$	Detailed energy balance, including contact angle (θ_a), and initial conditions
Ukiwe & Kwok (2005)	$(We+12)\beta = 8 + \beta^3\left(3(1-\cos\theta_d)+4\dfrac{We}{\sqrt{Re}}\right)$	Extension of the above model, with θ_d the dynamical contact angle during spreading
Clanet et al. (2004)	$\beta \propto We^{1/4}$	Mass balance using the impact capillary length
Roisman (2009)	$\beta \sim 0.87\,Re^{1/5} - 0.4\,Re^{2/5}\,We^{-1/2}$	Formula obtained using a dynamical model for the spreading of the drop involving a viscous boundary layer
Eggers et al. (2010)	$\beta = Re^{1/5}\,f(P)$	Similar approach to that in Roisman (2009); impact number P is defined by $P = We\,Re^{-2/5}$

that the correction due to the initial radius (typically leading one to consider $\beta - 1$ instead of β for the comparison for low Weber numbers) should be considered and would strongly lower the validity of this scaling. Quantitatively, as mentioned above, all these formulas eventually give good agreement with experimental and numerical data, so it is hard to discriminate between these different approaches. **Table 1** presents the most commonly used formulas in the literature to fit the experimental/numerical results.

Recently, dynamical models investigating the time evolution of a thin liquid film spreading on a solid substrate have provided a general framework for impact spreading that correctly describes the two regimes (viscous and inertial) and gives, in particular, a good understanding of the inertial regime, reconciling most of the existing models. Yarin & Weiss (1995) first proposed the use of the thin-film approximation in the investigation of the spreading dynamics after impact, and it was then adapted to different situations (Fedorchenko et al. 2005, Roisman 2009, Roisman et al. 2009, Eggers et al. 2010). A viscous boundary layer correction has recently been considered to the initial inviscid model, first by Roisman et al. (2009) and Roisman (2009) and later in a similar way by Eggers et al. (2010). The velocity in the spreading lamella can be described as a first approximation by the following inviscid hyperbolic axisymmetric velocity field:

$$v_r = \frac{r}{t} \quad \text{and} \quad v_z = -\frac{2z}{t}, \tag{3}$$

which corresponds to a decreasing pressure field with time (v_r and v_z being the radial and vertical velocities, respectively). Such flow suggests that in this regime, the drop surface [defined by $z = h(r, t)$] evolves in a self-similar way:

$$h(r, t) = \frac{1}{t^2}\,H\left(\frac{r}{t}\right), \tag{4}$$
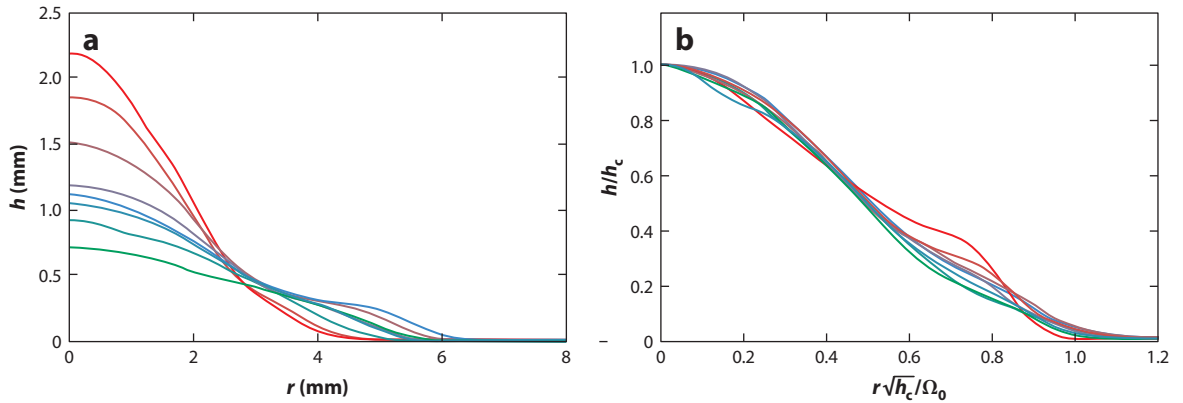
Figure 4

Experimental profile of a drop (*a*) impacting a solid surface at different times and (*b*) rescaled following Equation 4, where h_c is the central height of the interface and Ω_0 the square root of the drop volume. Figure adapted with permission from Lagubeau et al. (2012).

which has been observed both in numerical simulations (Roisman et al. 2009, Eggers et al. 2010) and in experiments (Lagubeau et al. 2012) (**Figure 4**).

However, such Eulerian flow (Equation 3) is not consistent with the no-slip boundary condition on the substrate, so a time-dependent viscous boundary layer develops from the substrate surface as the drop spreads. The thickness of this viscous layer obeys the usual scaling laws ($l_{bl} \sim \sqrt{\nu t}$), and accounting for its dynamics allows for a better understanding of the overall drop spreading. For example, the minimal liquid thickness experienced during the spreading (sometimes called, by extension, the residual thickness) is as follows:

$$h_{\min} \sim D \, Re^{-2/5}, \tag{5}$$

as observed numerically and experimentally (see **Figure 5a**) (Fedorchenko et al. 2005, Roisman 2009, Eggers et al. 2010, Lagubeau et al. 2012).

The spreading radius can be described through the value of an impact parameter $P_i = We \cdot Re^{-2/5}$, following

$$\beta = Re^{1/5} f_c(P_i). \tag{6}$$

The function f_c is expected to behave asymptotically as $P_i^{1/2}$ for small P_i and as a constant for large P_i, in agreement with the inertia-capillary and inertia-viscous balance, respectively. Although the inertia-capillary asymptotic limit cannot be investigated experimentally, this law confirms that it is the inertia-capillary balance that controls the spreading there ($\beta \propto We^{1/2}$) rather than the alternative one ($\beta \propto We^{1/4}$), as shown in **Figure 5b**, in which experiments with different liquids show a good collapse for the spreading factor according to Equation 6. Indeed, the latter law would have suggested another impact parameter $P_i' = We \cdot Re^{-4/5}$ for which the collapse of the results is clearly less good (Eggers et al. 2010, Laan et al. 2014, Lastakowski et al. 2014).

3.3. Impact on a Small Target

Impacts on small circular targets, the size of the drop itself, free the spreading lamella from the viscous no-slip boundary condition at the solid substrate, thus creating conditions closer to the above inviscid theory. This has been done in experiments by Rozhkov et al. (2010) and Villermaux & Bossa (2011) focusing on the puncturing of the lamella and fragmentation of its edge. Bakshi et al.
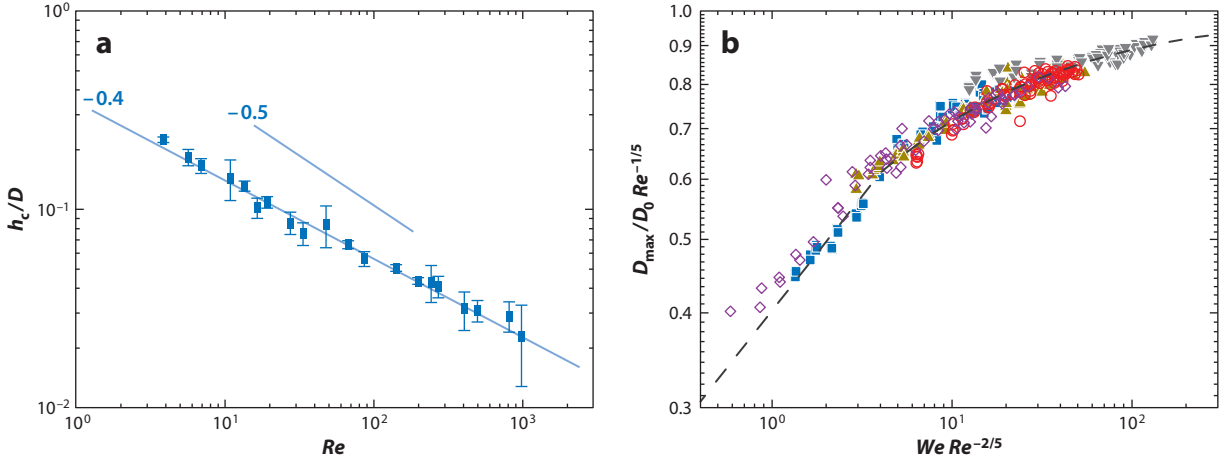
Figure 5

(*a*) Minimal film thickness during the drop impact, compared to the predicted $Re^{-2/5}$ law given in Equation 5. Panel *a* adapted with permission from Lagubeau et al. (2012). (*b*) Spreading factor measured for different liquids and impact velocities, traced following Equation 6. The dashed dark gray line represents the fit based on a Padé approximant according to the asymptotic limits $\lim_{P \ll 1} f_c(P) \propto P^{1/2}$ and $\lim_{P \gg 1} f_c(P) \sim$ cste. Panel *b* adapted with permission from Laan et al. (2014).

(2007) studied impacts on small spherical targets, varying the substrate curvature. Most recently, Vernay et al. (2015) measured the thickness of the free-standing sheet using fluorescence.

4. SPLASHING: PROMPT VERSUS CORONA SPLASH

4.1. Splashing Threshold

As the impact velocity V is increased, eventually the drop will splash (i.e., break up and eject smaller pieces). Classically, the splashing threshold was characterized by the so-called splashing parameter proposed by Stow & Hadfield (1981) and Mundo et al. (1995), which incorporated the inertia, viscous stress, and surface tension in the form

$$K = We\sqrt{Re}. \tag{7}$$

For impacts at $K \gtrsim 3,000$, one can expect a splash. Many variants of the above power laws exist in the literature (see review in Moreira et al. 2010 and Marengo et al. 2011). Motivated by the early imaging of Rioboo et al. (2001), the nature of the splash has been split into two categories, prompt and corona, shown in **Figure 1*d,e***, respectively. A prompt splash releases droplets directly from the breakup of the tip of the advancing lamella, whereas in the corona splash the intact lamella rises away from the substrate, forming a bowl-like structure, which subsequently breaks up into fine droplets. Much effort has been devoted to finding the critical values of K for various impact conditions (e.g., Vander Wal et al. 2006, Roisman et al. 2015).

4.2. Influence of the Surrounding Gas

The above formulation was proven to be incomplete by the unexpected discovery of Xu et al. (2005) that reducing the air pressure, while keeping other parameters unchanged, could suppress

splashing. This seminal discovery has triggered a renewed decade-long search for the underlying physics, in particular trying to pin down the role of air and the surface roughness (Tsai et al. 2009, 2010, 2011). As discussed below, many proposals have appeared, but consensus has yet to emerge.

The interplay between the surface roughness and gas pressure complicates the interpretation of the two splashing types. Xu et al. (2007) devised an ingenious way to study the size distribution of the ejected droplets by simply surrounding the impact with a circular sheet of paper. The resulting splatters showed different signatures for the two splashing types, with a thin horizontal line of spots for the prompt splash and a more vertically spread random distribution for the corona splash. However, this technique captured only forward-moving droplets and was limited to droplets larger than 100 μm. Direct imaging of the splashed droplets in the prompt splash regime showed that the earliest droplets are the smallest and emerge at the highest velocities, with early 5-μm droplets emerging at close to 90 m/s, or 10^4 times their terminal velocity (Thoroddsen et al. 2012) (see **Supplemental Video 1**). They are therefore rapidly decelerated by air drag and can easily become airborne. These observed droplet sizes support viscous growth of the thickness of the early lamella.

Xu et al. (2007) proposed that the prompt splash is produced by the surface roughness, whereas the corona splash is created by the air drag at the front of the lamella. This cannot be the whole story, as prompt microsplashing has been observed by Thoroddsen et al. (2012) for an impact on a smooth glass surface. Latka et al. (2012) proposed that perhaps a single mechanism is at play, simply appearing at different spreading locations. They removed the influence of the corona splash by conducting the experiments in a low-pressure helium atmosphere, clearly showing that a random surface roughness can reduce splashing by reducing the levitated film at the edge of the expanding lamella, while increasing prompt splashing.

Stevens et al. (2014) found an empirical scaling for the splashing boundary on a smooth surface using low-viscosity liquids over a range of gas pressures. The scaling highlights the importance of the mean-free path of the gas molecules.

A few studies have looked at splashing on inclined surfaces (Stow & Hadfield 1981) or rapidly translating surfaces. Chou et al. (2009) showed strong asymmetry and splashing even in the low–Weber number deposition regime, when the impact angle to the vertical direction exceeds 85°. Bird et al. (2009) additionally showed that the corona splash can be suppressed on the lamellar stretching side for a very large translational velocity of the substrate.

4.3. Levitated Lamella

The drop viscosity dramatically changes the splashing dynamics. For more viscous liquids, the lamella lifts away from the substrate (Driscoll et al. 2010, Schroll et al. 2010) and starts gliding on a thin sheet of air (**Figure 6a**). The forces responsible for the levitation of the sheet must arise from the dynamics around the rapidly moving contact line. Lubrication in the air under the sheet requires a large advancing contact angle, whereas suction in the airflow over the top is an inertial process. Bischofberger et al. (2013) introduced glycerin vapor into the air, forming spectacular Schlieren images (**Figure 6c**), to identify vortices forming above the leading edge of the lamella.

Thoroddsen et al. (2010) showed that this levitated lamella can become unstable and can touch the solid surface ahead of the contact line, thus not only entrapping a myriad of air bubbles when these localized contacts meet the expanding contact line (**Figure 6d**), but also rupturing the levitated lamella, producing a powerful capillary-driven splash. This bubble entrapment was studied in more detail by Driscoll et al. (2010) and Palacios et al. (2012), who observed multiple rings of microbubbles. The earliest breakup of the lamellar edge may be assisted by capillary instability in the cusp in the neck at which the lamella connects to the drop (**Figure 6b** and **Supplemental Video 2**) or by sawtooth instability at the contact line (Rein & Delplanque 2008).
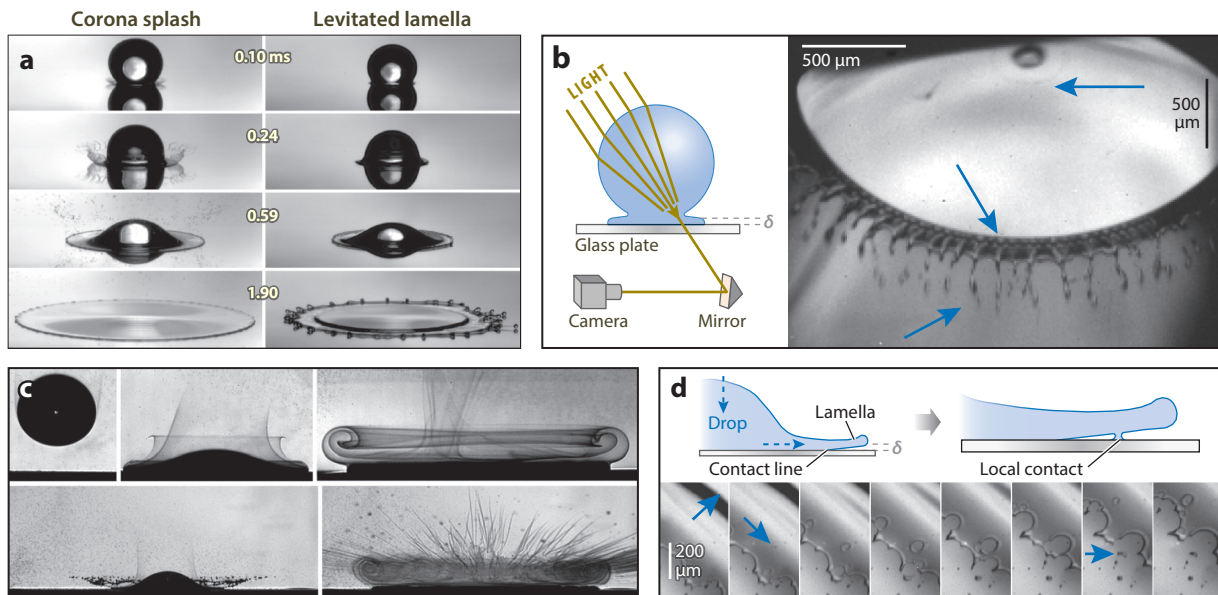
Figure 6

Splashing for different viscosities. (*a*) Comparison of splashing of a low- and high-viscosity liquid. Panel *a* adapted with permission from Driscoll et al. (2010). (*b*) Images demonstrating that splashing occurs as soon as the lamella appears from the outer wetted region, with an azimuthal pattern in the cusp. Panel *b* adapted with permission from Thoroddsen et al. (2012). (*c*) Visualization of the airflow using refractive index variations. Panel *c* taken with permission from Bischofberger et al. (2013). (*d*) Entrapment of bubbles under the contact line by localized contacts. Panel *d* adapted with permission from Thoroddsen et al. (2010). Readers are also referred to **Supplemental Videos 7–10**.

▶ Supplemental Material

Stevens et al. (2014) proposed that the delayed emergence of the thinner levitated jet from the tip of the lamella is a generic mechanism, occurring even for low-viscosity impacts. They quantified this time delay as a function of viscosity and air pressure. For the prompt splash, the first appearance of the lamella is thus emerging as a fundamental quantity, followed by the separation of its tip from the solid surface. However, immediately following the first wetting contact, the emergence of the lamella is controlled by the geometry of the drop, and it can splash instantaneously for low viscosities (e.g., see Thoroddsen et al. 2012 in which the droplet is shown to emerge immediately at a local tangential velocity to the lamellar tip motion). This was earlier studied by Mongruel et al. (2009) using multiple-strobe imaging and most recently by Riboux & Gordillo (2015).

4.4. Recent Theories

Riboux & Gordillo (2014) formulated a new splashing theory incorporating in part similar ideas for an impact on a smooth, partially wetting surface. They scaled the radial growth of the normalized wetted area as $r = \sqrt{3t}$, with fluid elements ejected at velocity $v_r = \sqrt{3/t}$. They proposed that the liftoff of the lamella has two contributions: the lubrication force of the air upstream of the contact line (arising a priori for a dynamic contact angle $>90°$) and the suction force due to the flow over the edge (given the Bernoulli inviscid mechanism there). The lubrication part depends on the contact angle and the mean-free path of the gas molecules, as already suggested in theoretical models involving noncontinuum gas correction (Duchemin & Josserand 2012, Mandre & Brenner

2012). Balancing the rising velocity of the tip of the ejecta with the capillary retraction Taylor-Culick velocity gives a splashing threshold that compares well with extensive data from Palacios et al. (2013), as well as with the reduced-pressure data from Xu et al. (2005), but does not include the influence of the surface wettability or roughness.

Liu et al. (2015) showed that a strategically placed ring of 75 μm through holes in the substrate can suppress splashing, whereas closed pits do not. This finding suggests that one needs to drain the air layer from under the outer edge to stabilize it. They proposed a Kelvin-Helmholtz instability at the interface between the thin air layer and the bottom of the drop as being responsible for the splashing, but they lacked direct imaging of the proposed instability. Lembach et al. (2010) have also shown a higher value for the splashing parameter for impacts on porous substrates. Alternatively, a splash can be triggered by an isolated protrusion, as shown by Josserand et al. (2005), or a pit, as shown by de Jong et al. (2015). Kim et al. (2014) tested impacts on various closed-pit morphologies, also invoking a Kelvin-Helmholtz instability to explain the lower critical values of the splashing parameter for larger pit areas.

Therefore, one can conclude that including the gas pressure in the splashing threshold must give rise to different scaling laws, as this effect is absent in the conventional splash parameter (Equation 7). In particular, varying the ambient gas pressure leads to a threshold such that the splashing is apparently enhanced by the gas viscosity (Stevens 2014, Stevens et al. 2014), suggesting that an overall criterion including all the parameters is still missing. This is also the conclusion of the recent work by Roisman et al. (2015) regarding critical values for the splashing parameter K (Equation 7). In particular, one should note that the incompressible lubrication equation for the gas cannot be enough to model the gas influence as it would involve only the Stokes number, which is independent from the gas pressure because of the Maxwell law (only the dynamical viscosity of the gas enters into the Stokes number). Thus, additional physical mechanisms, such as gas compressibility, inertia, and noncontinuum effects, have to be considered.

Finally, the above studies also highlight the difficulty in distinguishing between the prompt and corona splash, as exemplified by Riboux & Gordillo (2014), who showed that the separated lamella can stabilize by reattaching to the substrate. In fact, the splashing threshold based on the splashing parameter K (Equation 7) has been established without discriminating between the prompt and corona splash. Thus, an up-to-date parametric study separating these two dynamics is needed.

4.5. Fingering

The splat left behind after impact has a familiar fingering pattern (see **Figure 7**). The early work of Allen (1975) attributed the fingers to the Rayleigh-Taylor instability of the decelerating edge of the lamella, which has also been suggested by recent linear stability analysis of a liquid rim (Roisman et al. 2006, Agbaglah et al. 2013). However, clear fingering instability was observed from the very start of lamellar formation by Thoroddsen & Sakakibara (1998), who also showed that fingers can split and merge during spreading. Marmanis & Thoroddsen (1996) dropped colored liquids onto thick cotton paper, demonstrating that the number of fingers N scales with a modified impact Reynolds number $N \propto (Re_D^{1/2} We^{1/4})^{3/4}$. Aziz & Chandra (2000) proposed a different formula $N = Re^{1/4} We^{1/2}/\sqrt{48}$ for molten droplets. Mehdizadeh et al. (2004) extended these measurements to much higher impact velocities (~50 m/s) using a surface moving on a flywheel, which whacks the drop in flight. They showed reasonable scaling with the Weber number, $N = 1.14 We^{1/2}$, ignoring liquid viscosity. In the robust splashing regime, it becomes challenging to determine the number of fingers, as is clearly shown in the snapshots in **Figure 7b**. The same technique was used by Fassmann et al. (2013) to study the sizes of splashed droplets. Visser et al. (2012)
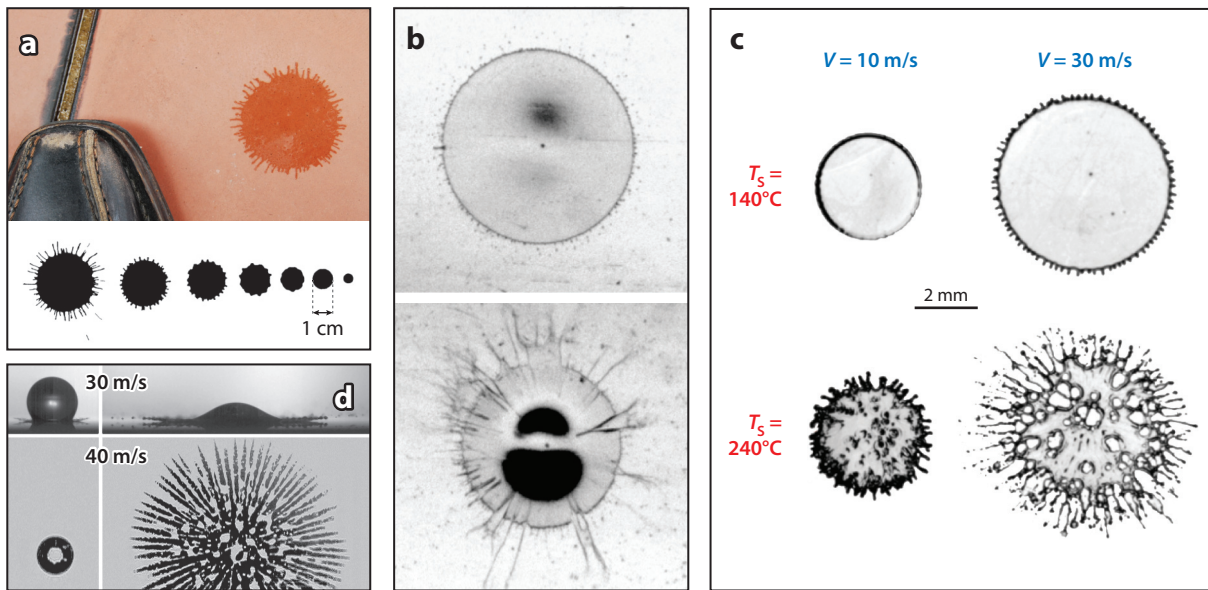
Figure 7

Splatter patterns. (*a*) The change in the numbers and shapes of fingering of an ink blot on paper when the impact height is increased. Panel *a* taken with permission from Marmanis & Thoroddsen (1996). (*b*) Edge splashing for very high impact velocities of 30 and 40 m/s. Panel *b* modified with permission from Mehdizadeh et al. (2004). (*c*) Drop smacked by a solid plate moving at up to 30 m/s, showing the effect of the surface superheat temperature. Panel *c* taken with permission from Mehdizadeh & Chandra (2006). (*d*) Fingering of vapor channels for a boiling drop on a heated surface. Panel *d* adapted with permission from Khavari et al. (2015).

achieved even higher impact velocities (∼100 m/s) of microdrops by exploiting laser-produced jetting (Thoroddsen et al. 2009). Impacts at huge Reynolds numbers have been studied by using larger liquid masses released from punctured balloons, but unavoidable external disturbances can obscure the impact-induced fingering (Yoon et al. 2007).

Blood-splatter analysis can be instrumental in forensic sciences (see Hulse-Smith et al. 2005, Laan et al. 2014). The combination of the diameter and number of fingers of the dried spatter can help pin down the droplet size and trajectory (see Attinger et al. 2013).

The splashing pattern itself obviously depends on the surface properties. At first, the wettability of the substrate is crucial for the splashing and breakup of the edge. The larger the contact angle, the easier is the splashing (Yokoi 2011) (**Figure 8**). Whereas the corona splash exhibits a typical S-shape ejecting small droplets, the skating thin film leads to the formation of fingers as shown in **Figure 8**.

5. THE EFFECTS OF SUBSTRATE PROPERTIES

Above we focus on impacts on flat dry surfaces. Allowing modification of the substrate opens up uncountable variants. The surface can be porous or compliant (Pepper et al. 2008, Gilet & Bourouiba 2014); one can add patterned roughness elements, penetrating holes, closed pits, or spatially varying wettability. Such modifications are a particularly active area of study, given the myriad of potential applications, from self-cleaning surfaces to enhanced heat transfer during spray cooling or anti-icing of airplane wings. This effort is aided by the rapid development of new micro- and nanofabrication techniques.
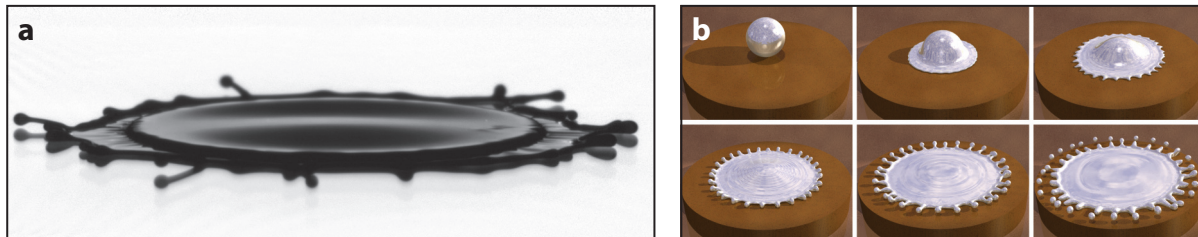
Figure 8

(*a*) Fingers and droplet breakup observed in the case of a liquid film skating on a solid surface. Panel *a* taken with permission from Driscoll & Nagel (2011). Fingering edge breakup obtained by direct numerical simulation. Panel *b* taken with permission from Yokoi (2011).

Motivated by the lotus leaf, superhydrophobic surfaces (i.e., hydrophobic and microstructured) have been engineered using various pillar arrangements to make an impacting fakir drop bounce with a restitution coefficient as high as 0.9 (Richard & Quéré 2000). In early studies, Reyssat et al. (2006) and Bartolo et al. (2006a) systematically varied the pillar height b and spacing ℓ to find the critical impact velocity V^* between the drop fully bouncing or partly wetting the surface (i.e., transitions from full to partial repellency). This transition occurs when the impact energy is sufficient to stretch the curved free meniscus between the pillars until they touch the substrate, giving

$$V^* = \sqrt{\delta b / \rho \ell^2}.$$

However, for even the most repellent surfaces at sufficiently high impact velocities, the spreading edge of the lamella will break up, and only part of the drop can rebound. van der Veen et al. (2014) used color interferometry to measure the shape of the meniscus between such pillars. Most recently, Antonini et al. (2014) applied X-rays to directly image the meniscus to pin down this wetting transition. Recent mushroom-shaped, double-reentrant, superomniphobic surfaces show bouncing of fully wettable liquids, such as hexadecane (Tuteja et al. 2008) and even perfluorohexane (Liu & Kim 2014).

Richard et al. (2002) demonstrated that the contact time of a drop impacting a smooth hydrophobic surface is almost constant, independent of the impact velocity, but grows linearly with drop size. Bird et al. (2013) showed that this time can be reduced by a cleverly constructed patterning of a superhydrophobic surface, which breaks the drop into smaller pieces. They suggested that some leaves and butterfly wings have developed such patterns. Moevius et al. (2014) demonstrated what they call a pancake rebound (**Figure 9***b*). This occurs when the impacting drop spreads along the texture but subsequently rebounds away from it before it can retract, thus retaining the flattened shape when the liquid leaves the surface. This has the possible advantage of further reducing the contact time of the drop with the substrate, which can be important in certain applications, such as anti-icing coatings. Coatings are also used to reduce bug-splatter remnants on windshields and airplane wings, on which impacts are usually at an angle (Yeong et al. 2014).

The next level of surface complexity involves modifications to promote directional rebounding, such as splitting the liquid into patterns or segmenting it onto wettable strips. Lee et al. (2010) studied impacts on a wettability-patterned surface, consisting of hydrophobized radial spikes, emanating from the center of the impact location (**Figure 9***c*). They successfully formed fine radial fingers at wavelengths different from the natural instability. Surprisingly, regular liquid patterns can be formed for both hydrophilic and hydrophobic line patterns, with the liquid resting on and in between the patterns, respectively. Reyssat et al. (2009) showed that variations of the
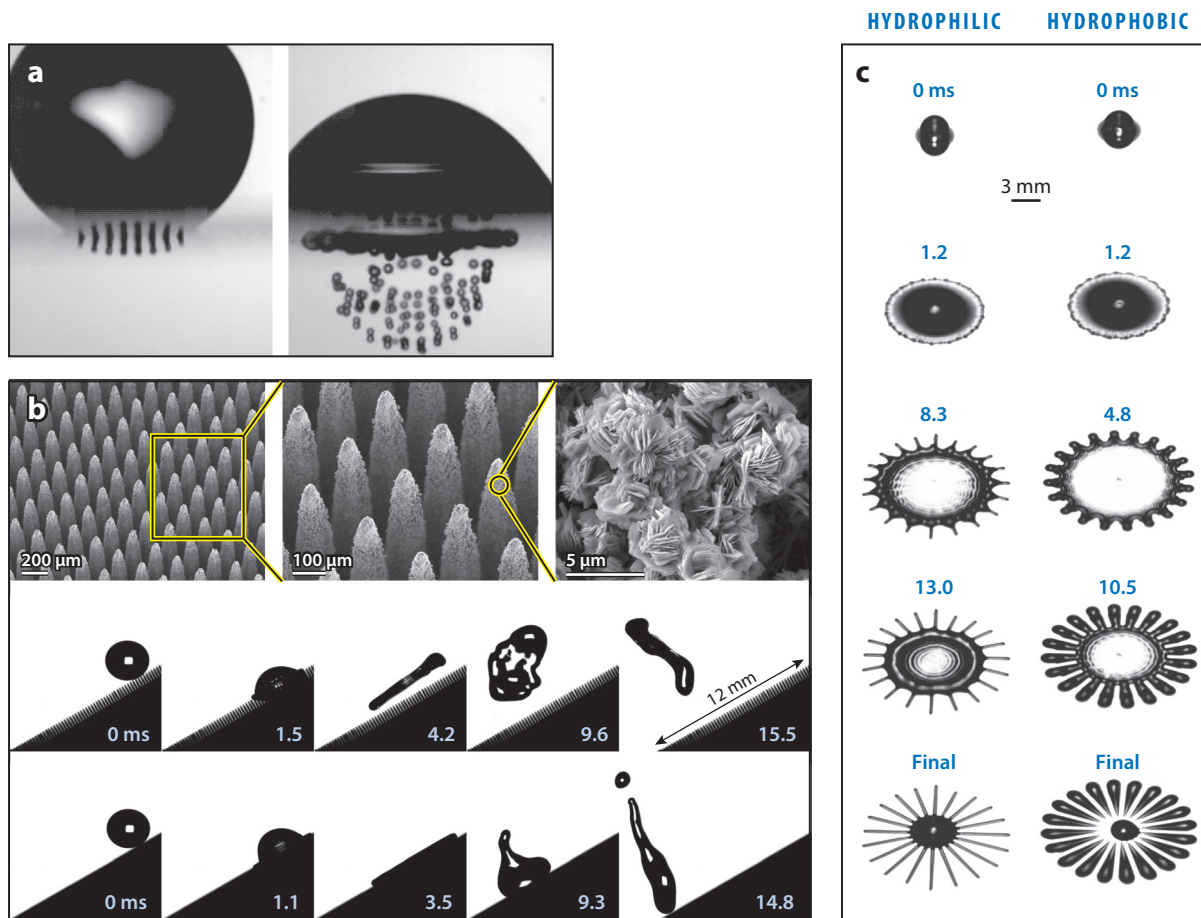
Figure 9

Shaping the splatter pattern. (*a*) Drop impacting on a regular grating ejecting smaller droplets. Panel *a* taken with permission from Brunet et al. (2009). (*b*) Pancake rebound from a superhydrophobic pillared surface. Panel *b* adapted with permission from Liu et al. (2014). (*c*) Impacts on radial patterns. In the left column, the radial lines are hydrophilic, whereas in the right column, they are hydrophobic. Panel *c* modified with permission from Lee et al. (2010).

postspacing along the surface can move the drops sideways. The impacting drops can also be formed into wetting patterns or can be redirected during the rebound (Schutzius et al. 2014).

Solid substrates can be porous or have isolated holes. Lorenceau & Quéré (2003) impacted a drop on a plate with a hole, identifying the critical *We* as function of *Re*, for which some of the liquid is ejected through the hole. Brunet et al. (2009) impacted a drop onto a regular microgrid, with holes in the form of truncated pyramids. The impact pushes through regular microdroplets with sizes similar to the individual hole size (**Figure 9a**). They demonstrated a larger critical *We* if the plate was turned over to form a reentrant surface structure. Similarly, Sahu et al. (2015) used porous mats of nanofibers, which have applications in heat exchangers. They saw fine jets emerging through the bottom of the mat, about three times faster than the drop impact velocity.

5.1. Phase Change During Impact

For certain applications, it is desired that the drop go through a phase change during impact. This can be solidification of a molten drop in soldering, or boiling of a drop during fuel-spray/wall interactions (Moreira et al. 2010), and in extreme spray cooling of electronic devices. Solidification is fundamental during inkjet soldering of electronics or fabrication of displays (Shinoda et al. 2009). Bhola & Chandra (1999) studied the solidification of paraffin wax, identifying the important parameters controlling the process. Aziz & Chandra (2000) examined the solidification and splashing of molten metal droplets, defining a solidification parameter and characterizing when solidification will not affect spreading.

Spray cooling can be most effective when it extracts heat into energy of vaporization of the spray droplets. Leidenfrost effects (Quéré 2013) are thus important, as they reduce heat transfer and enhance bouncing away from the substrate (Ko & Chung 1996). Biance et al. (2006) showed that Leidenfrost drops bounce with restitution coefficients exceeding unity, thus extracting energy from the vaporization. Antonini et al. (2013) demonstrated rebound due to the sublimation of a dry-ice substrate.

Moita & Moreira (2007) and Moreira et al. (2007) studied oils and petrochemicals fuels, showing jetting in the nucleate boiling regime. Breakup of the Leidenfrost layer under the drop has been studied by Tran et al. (2012) using interferometry. They identified explosive vertical jetting through the spreading lamella and characterized the splashing for heated surfaces, encompassing the Leidenfrost regime. Fingering of radial vapor lines during impact boiling was also observed in total internal reflection images under the drop, at temperatures slightly under the Leidenfrost point (**Figure 7d**) (Khavari et al. 2015).

5.2. Splashing of Composite Drops

Liquid suspensions and emulsions are ubiquitous in chemical processing and often form droplets. The impact of such droplets is thus of interest, for example, in spray cooling, lubrication, and combustion. Prunet-Foch et al. (1998) studied coolant/lubricant oil-water emulsions, sprayed on cold-rolling mills used in steel strip manufacturing. The impacts showed fine jetting, attributed to oil droplets ejected out of the free surface. **Figure 10** shows the impact of a drop containing large, heavier, internal perfluorohexane droplets, which settle near the bottom of the main drop. This forms isolated jets as the impact pressure field is focused around the internal smaller droplets, showing the importance of the number and location of the inner droplets. Counterjets have been observed during the impact of hollow drops (Gulyaev & Solonenko 2013).

The impact of dense suspensions of small solid particles has been imaged by Marston et al. (2013), showing grains ejected at twice the impact velocity of the granular drop. Peters et al. (2013) demonstrated that one should use a particle-based Weber number to predict the onset of splashing. Interestingly, for bimodal particles, the smaller ones are more readily ejected. Splashing of non-Newtonian liquids has thus far not been well studied (Guemas et al. 2009).

Naturally, research into the complex phenomenon of drop impact, focused first on the simplest configurations, has now shifted to fully attack the complexity of surface structure, complex-liquid drops, etc. Below are some of the issues that we believe need to be tackled. With accelerating improvements in both high-speed sensor technology and computational power, we expect the coming decade to provide even more breakthroughs in the study of drop impact, than have already occurred in the last decade since the review of Yarin (2006).
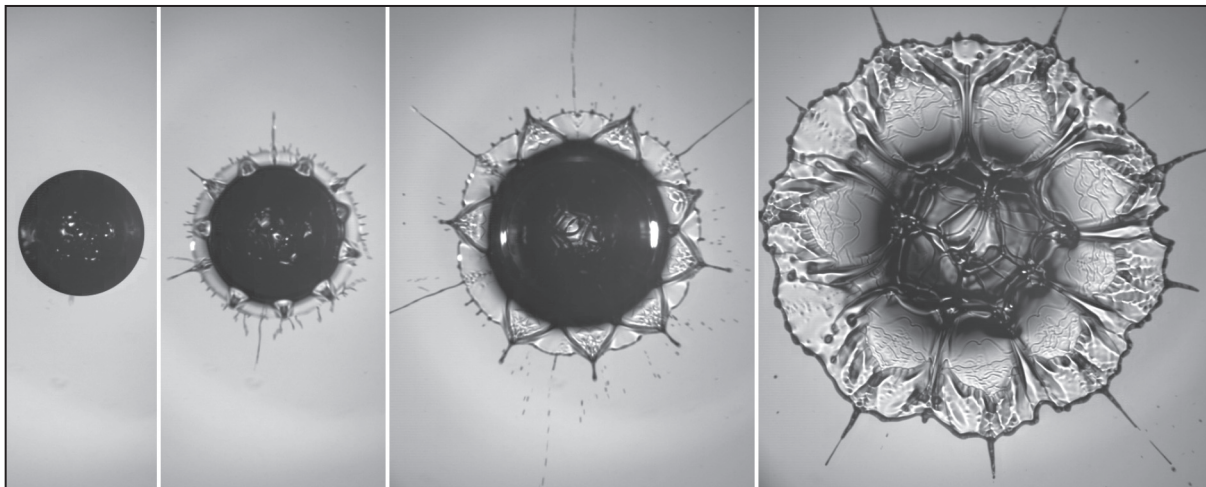
Figure 10

The impact of a compound drop, with outer drop of viscosity 2 cP and containing 20 inner PP1 droplets, for impact velocity $V \simeq 4$ m/s, drop $D \simeq 4$ mm. Frames are shown at $t = 0, 0.08, 0.25,$ and 0.8 ms after first contact. Note the repeatability of the fine structure. Readers are also referred to **Supplemental Video 11**. Figure courtesy of Jiaming Zhang & Erqiang Li.

▶ Supplemental Material

FUTURE ISSUES

1. Following the seminal discovery of Xu et al. (2005) that splashing is suppressed by reduced air pressure, many groups have tried to find the underlying mechanism. Numerous proposals have recently been put forth, some of which could be correct. The main focus is now on the levitation of the tip of the lamella as it travels along the substrate (Latka et al. 2012, Stevens et al. 2014, Riboux & Gordillo 2014, Liu et al. 2015). Improved imaging should pinpoint the most promising explanations for the different impact conditions to show whether a single unified splashing theory exists.

2. One uncertainty in this regard is the fuzzy definition of the splashing boundary, especially in the presence of surface roughness. Random roughness will inherently give random results, making it nontrivial to determine the splashing limit (e.g., see the large overlap of the splashing and deposition regimes observed in Roisman et al. 2015). High-speed microsplashing may also have been overlooked by early researchers (Thoroddsen et al. 2012). Furthermore, drops larger than the capillary length are easily deformed from the spherical shape, and air drag in free fall can flatten them. This invariable affects impact outcomes (Thoroddsen et al. 2005, Mishra et al. 2011, Liu et al. 2013) but was not characterized in many earlier studies.

3. Finding and predicting the splashing threshold are worthwhile quests in and of themselves. However, of greater practical importance will be to fully characterize the resulting splash. The size and number of the finest droplets are important, for example, for the generation of aerosols. Trajectories of droplets are important for the uniformity of coatings, contamination, or rain erosion.

4. Most experiments study only drop silhouettes, and numerics assume axisymmetry. Perhaps some instabilities reside in the flow field inside the drop, as has recently been shown numerically by Thoraval et al. (2012) for the drop-pool ejecta sheet. This poses fresh experimental challenges, which may be overcome in the near future.

5. The overwhelming majority of impact studies are far away from supersonic conditions (Lesser & Field 1983, Haller et al. 2002). However, such impacts can arise in applications such as sprays from high-pressure fuel injectors. Shock waves and the water-hammer pressure give rise to new dynamics. Direct measurements of the very large local forces involved might be possible with microscopic sensors. Overall forces can be measured using flexible glass substrates (Soto et al. 2014).

6. Practically, most impacts are oblique to the surface. This configuration deserves more attention.

7. Repeated drop impacts quickly wet the surface and transform the dynamics to impacts on liquid films, a topic not covered above, but even very thin films can have a strong effect on impact outcomes.

DISCLOSURE STATEMENT

ACKNOWLEDGMENTS

LITERATURE CITED

Agbaglah G, Delaux S, Fuster D, Hoepffner J, Josserand C, et al. 2011. Parallel simulation of multiphase flows using octree adaptivity and the volume-of-fluid method. *C. R. Mec.* 339:194–207

Agbaglah G, Josserand C, Zaleski S. 2013. Longitudinal instability of a liquid rim. *Phys. Fluids* 25:022103

Allen RF. 1975. The role of surface tension in splashing. *J. Colloid Interface Sci.* 51:350–51

Antkowiak A, Audoly B, Josserand C, Neukirch S, Rivetti M. 2011. Instant fabrication and selection of folded structures using drop impact. *PNAS* 108:10400–4

Antonini C, Bernagozzi I, Jung S, Poulikakos D, Marengo M. 2013. Water drops dancing on ice: how sublimation leads to drop rebound. *Phys. Rev. Lett.* 111:014501

Antonini C, Lee JB, Maitra T, Irvine S, Derome D, et al. 2014. Unraveling wetting transition through surface textures with X-rays: liquid meniscus penetration phenomena. *Sci. Rep.* 4:4055

Attinger D, Moore C, Donalson A, Jafari A, Stone HA. 2013. Fluid dynamics topics in bloodstain pattern analysis: comparative review and research opportunities. *Forensic Sci. Int.* 231:375–96

Aziz SD, Chandra S. 2000. Impact, recoil and splashing of molten metal droplets. *Int. J. Heat Mass Transf.* 43:2841–57

Bakshi S, Roisman IV, Tropea C. 2007. Investigations on the impact of a drop onto a small spherical target. *Phys. Fluids* 19:032102

Bartolo D, Bouamrirene F, Verneuil E, Buguin A, Silberzan P, Moulinet S. 2006a. Bouncing or sticky droplets: impalement transitions on superhydrophobic micropatterned surfaces. *Europhys. Lett.* 74:299–305

Bartolo D, Josserand C, Bonn D. 2005. Retraction dynamics of aqueous drops upon impact on nonwetting surfaces. *J. Fluid Mech.* 545:329–38

Bartolo D, Josserand C, Bonn D. 2006b. Singular jets and bubbles in drop impact. *Phys. Rev. Lett.* 96:124501

Bayer IS, Megaridis CM. 2006. Contact angle dynamics in droplets impacting on flat surfaces with different wetting characteristics. *J. Fluid Mech.* 558:415–49

Bhola R, Chandra S. 1999. Parameters controlling solidification of molten wax droplets falling on a solid surface. *J. Mater. Sci.* 34:4883–94

Biance A-L, Chevy F, Clanet C, Lagubeau G, Quéré D. 2006. On the elasticity of an inertial liquid shock. *J. Fluid Mech.* 554:47–66

Bird JC, Dhiman R, Kwon H-M, Varanasi KK. 2013. Reducing the contact time of a bouncing drop. *Nature* 503:385–88

Bird JC, Tsai S, Scott SH, Stone HA. 2009. Inclined to splash: triggering and inhibiting a splash with tangential velocity. *New J. Phys.* 11:063017

Bischofberger I, Mauser KW, Nagel SR. 2013. Seeing the invisible-air vortices around a splashing drop. *Phys. Fluids* 25:091110

Bouwhuis W, van der Veen RCA, Tran T, Keiji DL, Winkels KG, et al. 2012. Maximal air bubble entrainment at liquid-drop impact. *Phys. Rev. Lett.* 109:264501

Brunet P, Lapierre F, Zoueshtiagh F, Thomy V, Merlen A. 2009. To grate a liquid into tiny droplets by its impact on a hydrophobic microgrid. *Appl. Phys. Lett.* 95:254102

Chandra S, Avedisian CT. 1991. On the collision of a droplet with a solid surface. *Proc. R. Soc. A* 432:13–41

Chou F-C, Zen T-S, Lee K-W. 2009. An experimental study of a water droplet impacting on a rotating wafer. *Atom. Spray* 19:905–16

Clanet C, Béguin C, Richard D, Quéré D. 2004. Maximal deformation of an impacting drop. *J. Fluid Mech.* 517:199–208

de Jong R, Enriquez OR, van der Meer D. 2015. Exploring droplet impact near a millimetre-sized hole: comparing a closed pit with an open-ended pore. *J. Fluid Mech.* 772:427–44

de Ruiter J, Lagraauw R, van den Ende D, Mugele F. 2015a. Wettability-independent bouncing on flat surfaces mediated by thin air films. *Nat. Phys.* 11:48–53

de Ruiter J, Oh JM, van den Ende D, Mugele F. 2012. Dynamics of collapse of air films in drop impact. *Phys. Rev. Lett.* 108:074505

de Ruiter J, van den Ende D, Mugele F. 2015b. Air cushioning in droplet impact. II: Experimental characterization of the air film evolution. *Phys. Fluids* 27:012105

Deng X, Mammen L, Butt H-J, Vollmer D. 2012. Candle soot as a template for a transparent robust super-amphiphobic coating. *Science* 107:67–70

Driscoll MM, Nagel SR. 2011. Ultrafast interference imaging of air in splashing dynamics. *Phys. Rev. Lett.* 107:154502

Driscoll MM, Stevens CS, Nagel SR. 2010. Thin film formation during splashing of viscous liquids. *Phys. Rev. E* 83:036302

Duchemin L, Josserand C. 2011. Curvature singularity and film-skating during drop impact. *Phys. Fluids* 23:091701

Duchemin L, Josserand C. 2012. Rarefied gas correction for the bubble entrapment singularity in drop impacts. *C. R. Mec.* 340:797–803

Eggers J, Fontelos M, Josserand C, Zaleski S. 2010. Drop dynamics after impact on a solid wall: theory and simulations. *Phys. Fluids* 22:062101

Fassmann BW, Bansmer SE, Moeller TJ, Radespiel R, Hartmann M. 2013. High velocity impingement of single droplets on a dry smooth surface. *Exp. Fluids* 54:1516

Fedorchenko AI, Wang A-B, Wang Y-H. 2005. Effect of capillary and viscous forces on spreading of a liquid drop impinging on a solid surface. *Phys. Fluids* 17:093104

Gilet T, Bourouiba L. 2014. Rain-induced ejection of pathogens from leaves: revisiting the hypothesis of splash-on-film using high-speed visualization. *Integr. Comp. Biol.* 54:974–84

Guemas M, Marin AG, Lohse D. 2009. Drop impact experiments of non-Newtonian liquids on micro-structured surfaces. *Soft Matter* 8:10725–31

Gulyaev IP, Solonenko OP. 2013. Hollow droplets impacting onto a solid surface. *Exp. Fluids* 54:1432

Haller KK, Ventikos Y, Poulikakos D, Monkewitz P. 2002. Computational study of high-speed liquid droplet impact. *J. Appl. Phys.* 92:2821–28

Hendrix MHW, Bouwhuis W, van der Meer D, Lohse D, Snoeijer JH. 2015. Universal mechanism for air entrainment during liquid impact.. arXiv:1502.02869v1 [physics.flu-dyn]

Hicks PD, Ermanyuk EV, Gavrilov NV, Purvis R. 2012. Air trapping at impact of a rigid sphere onto a liquid. *J. Fluid Mech.* 695:310–20

Hicks PD, Purvis R. 2010. Air cushioning and bubble entrapment in three-dimensional droplet impacts. *J. Fluid Mech.* 649:135–63

Hicks PD, Purvis R. 2013. Liquid-solid impacts with compressible gas cushioning. *J. Fluid Mech.* 735:120–49

Huang Y-L, Wang M-J, Huang J-W, Lin S-Y. 2013. A study on the impact velocity and drop size for the occurrence of entrapped air bubbles: water on parafilm. *Exp. Therm. Fluid Sci.* 48:102–9

Hulse-Smith L, Mehdizadeh NZ, Chandra S. 2005. Deducing drop size and impact velocity from circular bloodstains. *J. Forensic Sci.* 50:54–63

Josserand C, Lemoyne L, Troeger R, Zaleski S. 2005. Droplet impact on a dry surface: triggering the splash with a small obstacle. *J. Fluid Mech.* 524:47–56

Joung YS, Buie CR. 2015. Aerosol generation by raindrop impact on soil. *Nat. Commun.* 6:6083

Khavari M, Sun C, Lohse D, Tran T. 2015. Fingering patterns during droplet impact on heated surfaces. *Soft Matter* 11:3298–303

Kim H, Park U, Lee C, Kim H, Kim MH, Kim J. 2014. Drop splashing on a rough surface: how surface morphology affects splashing threshold. *Appl. Phys. Lett.* 104:161608

Klaseboer E, Chevaillier JP, Gourdon C, Masbernat O. 2000. Film drainage between colliding drops at constant approach velocity: experiments and modeling. *J. Colloid Interface Sci.* 229:274–85

Klaseboer E, Manica R, Chan DYC. 2014. Universal behavior of the initial stage of drop impact. *Phys. Rev. Lett.* 113:194501

Ko YS, Chung SH. 1996. An experiment on the breakup of impinging droplets on a hot surface. *Exp. Fluids* 21:118–23

Kolinski JM, Rubinstein SM, Mandre S, Brenner MP, Weitz DA. 2012. Skating on a film of air: drops impacting on a surface. *Phys. Rev. Lett.* 108:074503

Kolinski JM, Mahadevan L, Rubinstein SM. 2014a. Drops can bounce from perfectly hydrophilic surfaces. *Eur. Phys. Lett.* 108:24001

Kolinski JM, Mahadevan L, Rubinstein SM. 2014b. Lift-off instability during the impact of a drop on a solid surface. *Phys. Rev. Lett.* 112:134501

Korobkin AA, Ellis AS, Smith FT. 2008. Trapping of air in impact between a body and shallow water. *J. Fluid Mech.* 611:365–94

Kwon D, Huh H, Lee S. 2013. Wetting state and maximum spreading factor of microdroplets impacting on superhydrophobic textured surfaces with anisotropic arrays of pillars. *Exp. Fluids* 54:1576

Laan N, de Bruin KG, Bartolo D, Josserand C, Bonn D. 2014. Maximum diameter of impacting liquid droplets. *Phys. Rev. Appl.* 2:044018

Lagubeau G, Fontelos MA, Josserand C, Maurel A, Pagneux V, Petitjeans P. 2012. Spreading dynamics of drop impacts. *J. Fluid Mech.* 713:50–60

Lastakowski H, Boyer F, Biance A-L, Pirat C, Ybert C. 2014. Bridging local to global dynamics of drop impact onto solid substrates. *J. Fluid Mech.* 747:103–18

Latka A, Strandburg-Peshkin A, Driscoll MM, Stevens CS, Nagel SR. 2012. Creation of prompt and thin-sheet splashing by varying surface roughness or increasing air pressure. *Phys. Rev. Lett.* 109:054501

Lee JS, Weon BM, Je JH, Fezzaa K. 2012. How does an air film evolve into a bubble during drop impact? *Phys. Rev. Lett.* 109:204501

Lee M, Chang YS, Kim H-Y. 2010. Drop impact on microwetting patterned surfaces. *Phys. Fluids* 22:072101

Lembach AN, Tan H-B, Roisman IV, Gambaryan-Roisman T, Zhang Y, et al. 2010. Drop impact, spreading, splashing, and penetration into electrospun nanofiber mats. *Langmuir* 26:9516–23

Lesser M, Field JE. 1983. The impact of compressible liquids. *Annu. Rev. Fluid Mech.* 15:97–122

Li EQ, Thoroddsen ST. 2015. Time-resolved imaging of a compressible air-disc under a drop impacting on a solid surface. *J. Fluid Mech.* 780:636–48

Liu TL, Kim CJ. 2014. Turning a surface superrepellent even to completely wetting liquids. *Science* 346:1096–100

Liu Y, Moevius L, Xu X, Qian T, Yeomans JM, Wang Z. 2014. Pancake bouncing on superhydrophobic surfaces. *Nat. Phys.* 10:515–19

Liu Y, Tan P, Xu L. 2013. Compressible air entrapment in high-speed drop impacts on solid surfaces. *J. Fluid Mech.* 716:R9

Liu Y, Tan P, Xu L. 2015. Kelvin–Helmholtz instability in an ultrathin air film causes drop splashing on smooth surfaces. *PNAS* 112:3280–84

Lorenceau E, Quéré D. 2003. Drop impacting a sieve. *J. Colloid Interface Sci.* 263:244–49

Maitra T, Tiwari MK, Antonin C, Schoch P, Jung S, et al. 2014. On the nanoengineering of superhydrophobic and impalement resistant surface textures below the freezing temperature. *Nano Lett.* 14:172–82

Mandre S, Brenner MP. 2012. The mechanism of a splash on a dry solid surface. *J. Fluid Mech.* 690:148–72

Mandre S, Mani M, Brenner MP. 2009. Precursors to splashing of liquid droplets on a solid surface. *Phys. Rev. Lett.* 102:134502

Mani M, Mandre S, Brenner MP. 2010. Events before droplet splashing on a solid surface. *J. Fluid. Mech.* 647:163–85

Marengo M, Antonini C, Roisman IV, Tropea C. 2011. Drop collisions with simple and complex surfaces. *Curr. Opin. Colloid Interface Sci.* 16:292–302

Marmanis H, Thoroddsen ST. 1996. Scaling of the fingering pattern of an impacting drop. *Phys. Fluids* 8:1344–46

Marston JO, Mansoor MM, Thoroddsen ST. 2013. Impact of granular drops. *Phys. Rev. E* 88:010201

Marston JO, Vakarelski IU, Thoroddsen ST. 2011. Bubble entrapment during sphere impact onto quiescent liquid surfaces. *J. Fluid Mech.* 680:660–70

Mehdizadeh NZ, Chandra S. 2006. Boiling during high-velocity impact of water droplets on a hot stainless steel surface. *Proc. R. Soc. A* 462:3115–31

Mehdizadeh NZ, Chandra S, Mostaghimi J. 2004. Formation of fingers around the edges of a drop hitting a metal plate with high velocity. *J. Fluid Mech.* 510:353–73

Minemawari H, Yamada T, Matsui H, Tsutsumi J, Haas S, et al. 2011. Inkjet printing of single-crystal films. *Nature* 475:364–67

Mishra NK, Zhang Y, Ratner A. 2011. Effect of chamber pressure on spreading and splashing of liquid drops upon impact on a dry smooth stationary surface. *Exp. Fluids* 51:483–91

Moevius L, Liu Y, Wang Z, Yeomans JM. 2014. Pancake bouncing: simulations and theory and experimental verification. *Langmuir* 30:13021–32

Moita AS, Moreira ALN. 2007. Drop impacts onto cold and heated rigid surfaces: morphological comparisons, disintegration limits and secondary atomization. *Int. J. Heat Fluid Flow* 28:735–52

Mongruel A, Daru V, Feuillebois F, Tabakova SS. 2009. Early post-impact time dynamics of viscous drops onto a solid dry surface. *Phys. Fluids* 21:032101

Moreira ALN, Moita AS, Cossali E, Marengo M, Santini M. 2007. Secondary atomization of water and isooctane drops impinging on tilted heated surfaces. *Exp. Fluids* 43:297–313

Moreira ALN, Moita AS, Panão MR. 2010. Advances and challenges in explaining fuel spray impingement: How much of single droplet impact research is useful? *Prog. Energy Combust. Sci.* 36:554–80

Mundo C, Sommerfeld M, Tropea C. 1995. Droplet-wall collisions: experimental studies of the deformation and breakup process. *Int. J. Multiphase Flow* 21:151–73

Palacios J, Hernández J, Gómez P, Zanzi C, López J. 2012. On the impact of viscous drops onto dry smooth surfaces. *Exp. Fluids* 52:1449–63

Palacios J, Hernández J, Gómez P, Zanzi C, López J. 2013. Experimental study of splashing patterns and the splashing/deposition threshold in drop impacts onto dry smooth solid surfaces. *Exp. Therm. Fluid Sci.* 44:571–82

Pasandideh-Fard M, Qiao YM, Chandra S, Mostaghimi J. 1996. Capillary effects during droplet impact on a solid surface. *Phys. Fluids* 8:650–59

Pepper RE, Courbin L, Stone HA. 2008. Splashing on elastic membranes: the importance of early-time dynamics. *Phys. Fluids* 20:082103

Peters IR, Xu Q, Jaeger HM. 2013. Splashing onset in dense suspension droplets. *Phys. Rev. Lett.* 111:028301

Piroird K, Clanet C, Lorenceau E, Quéré D. 2009. Drops impacting inclined fibers. *J. Colloid Interface Sci.* 334:70–74

Pittoni PG, Lin Y-C, Wang R-J, Yu T-S, Lin S-Y. 2015. Bubbles entrapment for drops impinging on polymer surfaces: the roughness effect. *Exp. Therm. Fluid Sci.* 62:183–91

Prunet-Foch B, Legay F, Vignes-Adler M, Delmotte C. 1998. Impacting emulsion drop on a steel plate: influence of the solid substrate. *J. Colloid Interface Sci.* 199:151–68

Quéré D. 2013. Leidenfrost dynamics. *Annu. Rev. Fluid Mech.* 45:197–215

Range K, Feuillebois F. 1998. Influence of surface roughness on liquid drop impact. *J. Colloid Interface Sci.* 203:16–30

Rein M. 1993. Phenomena of liquid drop impact on solid and liquid surfaces. *Fluid Dyn. Res.* 12:61–93

Rein M, Delplanque J-P. 2008. The role of air entrainment on the outcome of drop impact on a solid surface. *Acta Mech.* 201:105–18

Renardy Y, Popinet S, Duchemin L, Renardy M, Zaleski S, et al. 2003. Pyramidal and toroidal water drops after impact on a solid surface. *J. Fluid Mech.* 484:69–83

Reyssat M, Pardo F, Quéré D. 2009. Drops onto gradients of texture. *Europhys. Lett.* 87:36003

Reyssat M, Pepin A, Marty F, Chen Y, Quéré D. 2006. Bouncing transitions on microtextured materials. *Europhys. Lett.* 74:306–12

Riboux G, Gordillo JM. 2014. Experiments of drops impacting a smooth solid surface: a model of the critical impact speed for drop splashing. *Phys. Rev. Lett.* 113:024507

Riboux G, Gordillo JM. 2015. The diameter and velocities of the droplets ejected after splashing. *J. Fluid Mech.* 772:630–48

Richard D, Clanet C, Quéré D. 2002. Contact time of a bouncing drop. *Nature* 417:811

Richard D, Quéré D. 2000. Bouncing water drops. *Europhys. Lett.* 50:769–75

Rioboo R, Marengo M, Tropea C. 2002. Time evolution of liquid drop impact onto solid, dry surfaces. *Exp. Fluids* 33:112–24

Rioboo R, Tropea C, Marengo M. 2001. Outcomes from a drop impact on solid surfaces. *At. Sprays* 11:155–65

Roisman IV. 2009. Inertia dominated drop collisions. II. An analytical solution of the Navier-Stokes equations for a spreading viscous film. *Phys. Fluids* 21:052104

Roisman IV, Berberović E, Tropea C. 2009. Inertia dominated drop collisions. I. On the universal flow in the lamella. *Phys. Fluids* 21:052103

Roisman IV, Horvat K, Tropea C. 2006. Spray impact: rim transverse instability initiating fingering and splash and description of a secondary spray. *Phys. Fluids* 18:102104

Roisman IV, Lembach A, Tropea C. 2015. Drop splashing induced by target roughness and porosity: The size plays no role. *Adv. Colloid Interface Sci.* 222:615–21

Roisman IV, Rioboo R, Tropea C. 2002. Normal impact of a liquid drop on a dry surface: model for spreading and receding. *Proc. R. Soc. A* 458:1411–30

Rozhkov A, Brunet-Foch B, Vignes-Adler M. 2010. Impact of drops of surfactant solutions on small targets. *Proc. R. Soc. A* 466:2897–916

Sahu RP, Sett S, Yarin AL, Pourdeyhimi B. 2015. Impact of aqueous suspension drops onto non-wettable porous membranes: hydrodynamic focusing and penetration of nanoparticles. *Colloids Surf. A* 467:31–45

Scheller BL, Bousfield DW. 1995. Newtonian drop impact with a solid surface. *AIChE J.* 41:1357–67

Schroll RD, Josserand C, Zaleski S, Zhang WW. 2010. Impact of a viscous liquid drop. *Phys. Rev. Lett.* 104:034504

Schutzius TM, Graeber G, Elsarkawy M, Oreluk J, Megaridis CM. 2014. Morphing and vectoring impacting droplets by means of wettability-engineered surfaces. *Sci. Rep.* 4:7029

Shinoda K, Raessi M, Mostaghimi J, Yoshida T, Murakami H. 2009. Effect of substrate concave pattern on splat formation of yttria-stabilized zirconia in atmospheric plasma spraying. *J. Therm. Spray Technol.* 18:609–18

Smith FT, Li L, Wu GX. 2003. Air cushioning with a lubrication/inviscid balance. *J. Fluid Mech.* 482:291–318

Soto D, De Larivière AB, Boutillon X, Clanet C, Quéré D. 2014. The force of impacting rain. *Soft Matter* 10:4929–34

Stevens CS. 2014. Scaling of the splash threshold for low-viscosity fluids. *Eur. Phys. Lett.* 106:24001

Stevens CS, Latka A, Nagel SN. 2014. Comparison of splashing in high- and low-viscosity liquids. *Phys. Rev. E* 89:063006

Stow CD, Hadfield MG. 1981. An experimental investigation of fluid flow resulting from the impact of a water drop with an unyielding dry surface. *Proc. R. Soc. A* 373:419–41

Thoraval M-J, Takehara K, Etoh TG, Popinet S, Ray P, et al. 2012. Von Kármán vortex street within an impacting drop. *Phys. Rev. Lett.* 108:264506

Thoroddsen ST, Etoh TG, Takehara K. 2008. High-speed imaging of drops and bubbles. *Annu. Rev. Fluid Mech.* 40:257–85

Thoroddsen ST, Etoh TG, Takehara K, Ootsuka N, Hatsuki Y. 2005. The air bubble entrapped under a drop impacting on a solid surface. *J. Fluid Mech.* 545:203–12

Thoroddsen ST, Takehara K, Etoh TG. 2010. Bubble entrapment through topological change. *Phys. Fluids* 22:051701

Thoroddsen ST, Takehara K, Etoh TG. 2012. Micro-splashing by drop impacts. *J. Fluid Mech.* 706:560–70

Thoroddsen ST, Takehara K, Etoh TG, Ohl C-D. 2009. Spray and microjets produced by focusing a laser pulse into a hemispheric drop. *Phys. Fluids* 21:112101

Thoroddsen ST, Sakakibara J. 1998. Evolution of the fingering pattern of an impacting drop. *Phys. Fluids* 10:1359–74

Tran T, Staat HJJ, Prosperetti A, Sun C, Lohse D. 2012. Drop impact on superheated surfaces. *Phys. Rev. Lett.* 108:036101

Tsai PA, Hendrix MHW, Dijkstra RRM, Shui L, Lohse D. 2011. Microscopic structure influencing macroscopic splash at high Weber number. *Soft Matter* 7:11325–33

Tsai PA, Pacheco S, Pirat C, Lefferts L, Lohse D. 2009. Drop impact upon micro- and nanostructured superhydrophobic surfaces. *Langmuir* 25:12293–98

Tsai PA, van der Veen RCA, van de Raa M, Lohse D. 2010. How micropatterns and air pressure affect splashing on surfaces. *Langmuir* 26:16090–95

Tuteja A, Choi W, Mabry JM, McKinley GH, Cohen RE. 2008. Robust omniphobic surfaces. *PNAS* 105:18200–5

Ukiwe C, Kwok D. 2005. On the maximum spreading diameter of impacting droplets on well-prepared solid surfaces. *Langmuir* 21:666–73

Vadillo D, Soucemarianadin A, Delattre C, Roux D. 2009. Dynamic contact angle effects onto the maximum drop impact spreading on solid surfaces. *Phys. Fluids* 21:122002

Van Dam DB, Le Clerc C. 2004. Experimental study of the impact of an ink-jet printed droplet on a solid substrate. *Phys. Fluids* 16:3403–14

van der Veen RCA, Tran T, Lohse D, Sun C. 2012. Direct measurements of air layer profiles under impacting droplets using high-speed color interferometry. *Phys. Rev. E* 85:026315

van der Veen RCA, Hendrix MHW, Tran T, Sun C, Tsai PA, Lohse D. 2014. How microstructures affect air film dynamics prior to drop impact. *Soft Matter* 10:3703–7

Vander Wal RL, Berger GM, Mozes SD. 2006. The splash/non-splash boundary upon a dry surface and thin fluid film. *Exp. Fluids* 40:53–59

Vernay C, Ramos L, Ligoure C. 2015. Free radially expanding liquid sheet in air: time- and space-resolved measurement of the thickness field. *J. Fluid Mech.* 764:428–44

Villermaux E, Bossa B. 2011. Drop fragmentation on impact. *J. Fluid Mech.* 668:412–35

Visser CW, Frommhold PE, Wildeman S, Mettin R, Lohse D, Sun C. 2015. Dynamics of high-speed microdrop impact: numerical simulations and experiments at frame-to-frame times below 100 ns. *Soft Matter* 11:1708–22

Visser CW, Tagawa Y, Sun C, Lohse D. 2012. Microdroplet impact at very high velocity. *Soft Matter* 8:10732–37

Worthington AM. 1876. On the forms assumed by drops of liquids falling vertically on a horizontal plate. *Proc. R. Soc.* 25:261–72

Xu L, Barcos L, Nagel SR. 2007. Splashing of liquids: interplay of surface roughness with surrounding gas. *Phys. Rev. Lett.* 76:066311

Xu L, Zhang WW, Nagel SR. 2005. Drop splashing on a dry smooth surface. *Phys. Rev. Lett.* 94:184505

Yarin AL. 2006. Drop impact dynamics: splashing, spreading, receding, bouncing. *Annu. Rev. Fluid Mech.* 38:159–92

Yarin AL, Weiss DA. 1995. Impact of drops on solid surfaces: self-similar capillary waves, and splashing as a new type of kinematic discontinuity. *J. Fluid Mech.* 283:141–73

Yeong YH, Burton J, Loth E, Bayer IS. 2014. Drop impact and rebound dynamics on an inclined superhydrophobic surface. *Langmuir* 30:12027–38

Yokoi K. 2011. Numerical studies of droplet splashing on a dry surface: triggering a splash with the dynamic contact angle. *Soft Matter* 7:5120–23

Yokoi K, Vadillo D, Hinch J, Hutchings I. 2009. Numerical studies of the influence of the dynamic contact angle on a drop impacting on a dry surface. *Phys. Fluids* 21:072102

Yoon SS, Jepsen RA, Nissen MR, O'Hern TJ. 2007. Experimental investigation on splashing and nonlinear fingerlike instability of large water drops. *J. Fluids Struct.* 23:101–15